Investigation of the Level Structure of $^{91-94}$Zr Nuclei Using Large-Scale Shell-Model Calculations*

Bin-Ran Tan (谭彬然)[1] Hao-Yu Jiang (江昊宇)[1] H. K. Wang (王韩奎)[1†] Zhi-Hong Li (李志宏)[2,3‡]

[1]Department of Physics, Zhejiang SCI-TECH University, Hangzhou 310018, China
[2]China Institute of Atomic Energy, P.O. Box 275(10), Beijing 102413, China
[3]School of Nuclear Science and Technology, University of Chinese Academy of Sciences, Beijing 101408, China

Abstract: A suitable Hamiltonian is designed for the Zr isotopes over the N = 50 shell by including shell model space between ^{78}Ni and ^{132}Sn. The Hamiltonian is composed by the pairing-plus-multipole force and monopole correction terms. The single-particle energies (SPEs) are initially taken from the low-lying states of the hole nuclei ^{131}In and ^{131}Sn (near the N=82 shell closure). These SPEs are then modified by three monopole correction terms to better describe the low-lying states of ^{91}Zr (near the N=50 shell closure). To test this Hamiltonian, the level spectra of $^{91-94}$Zr are investigated in both low-lying and high-spin excitations by large-scale shell-model calculations. Their wave functions are further tested by comparing the electromagnetic transition probabilities with given $B(E2)$ data. The good performance in both spectra and transitions probabilities makes the predicting calculations of the present interaction more dependable to be referred in further experimental researches of Zr isotopes.

Keywords: Level structure, Shell model, Monopole correction, Electromagnetic transitions

DOI: **CSTR:**

I. INTRODUCTION

The nuclei region around mass number A = 90 lies close to the first abundance peak of the rapid neutron-capture process (r-process)[1−5]. Key nuclei in this region, such as ^{90}Zr, and ^{90}Mo, play a crucial role in nucleosynthesis networks[6−12]. Their nuclear properties, including masses[13, 14], lifetimes[15−17], and neutron-capture cross-sections[18, 19], directly influence the accuracy of r-process simulations, thereby shaping our understanding of the origin of heavy elements in the universe, particularly in astrophysical events such as neutron-star mergers[20−22].

Zirconium isotopes are of particular importance across multiple disciplines, including nuclear physics, astrophysics, nuclear energy, and geochemistry. Their unique nuclear behavior and chemical stability make them a focal point for both fundamental and applied research. In nuclear energy applications, natural zirconium, composed predominantly of ^{90}Zr, ^{91}Zr, ^{93}Zr, ^{94}Zr, exhibits an exceptionally low thermal-neutron capture cross-section[18, 23−25]. This property renders zirconium alloys the material of choice for fuel-rod cladding and structural components in light-water reactors[26]. Furthermore, ^{95}Zr, a medium-lived fission product (half-life about 64 days), serves as an important monitor of fuel burn-up and fission yield in reactor operations and nuclear tests[27]. Several long-lived radioactive zirconium isotopes also appear in nuclear waste streams, and research into their nuclear properties supports the assessment of waste inventories and the development of potential transmutation strategies[28].

From a nuclear-structure perspective, zirconium isotopes span a critical region of the nuclear chart. The isotope ^{90}Zr, with a neutron number N = 50, corresponds to a traditional neutron shell closure. Systematic studies from neutron-deficient species (e.g., ^{80}Zr) to neutron-rich ones (e.g., ^{110}Zr) reveal the evolution of nuclear shell structure[30, 31], the onset of collective deformation[32, 33], and the occurrence of shape coexistence[34−36]. While traditional shell models predict N = 50 as a magic number associated with spherical closed shells, experimental evidence indicates significant deformation in many nuclides near this region, reflecting the weakening of magic effects and the evolution of shell structure[37−39].

In this work, a suitable shell model interaction is designed for describing the level structure of Zr isotopes (A >90) in both low-lying and high-spin excitations. This in-

Received 1 January 2026; Accepted 9 February 2026

* Research at ZSTU was supported by the National Natural Science Foundation of China (Grants No.12475124, No.U2267205), and ZSTU intramural grant(22062267-Y). Research at China Institute of Atomic Energy was supported by the National Natural Science Foundation of China (Grants No. 12475151)

† E-mail: whk@zstu.edu.cn
‡ E-mail: zhli@ciae.ac.cn

teraction includes the pairing-plus-multipole force and the monopole corrections in the shell model space with four proton and five neutron orbits between ^{78}Ni and ^{132}Sn. The next section **2** gives the interaction model framework. Sec. **3** shows its performance in the level spectra of nuclei $^{91-94}$Zr, as well as Electromagnetic Transitions probabilities. Sec. **4** presents the conclusions. The shell-model code NUSHELL@MSU is used for the calculations [40].

II. HAMILTONIAN

The shell model space includes five neutron levels below the neutron magic number $N = 82$ ($0g_{7/2}$, $1d_{5/2}$, $2s_{1/2}$, $0h_{11/2}$, $1d_{3/2}$) and four proton levels below the proton magic number $N = 50$ ($0f_{5/2}$, $1p_{3/2}$, $1p_{1/2}$, $0g_{9/2}$), with the frozen core ^{78}Ni. The single particle states of these orbits are referred from Ref[41], which selected from the low-lying levels of single hole nuclei ^{131}In and ^{131}Sn under the ^{132}Sn. The Hamiltonian of this model space is given in the proton-neutron (pn) representation as following:

$$\begin{aligned} H &= H_{SP} + H_{P_0} + H_{P_2} + H_{QQ} + H_{OO} + H_{HH} + H_{mc} \\ &= \sum_{\alpha,i} \epsilon_a^i c_{\alpha,i}^\dagger c_{\alpha,i} - \frac{1}{2}\sum_{I=0,2}\sum_{ii'} g_I, ii' \sum_M P_{IM,ii'}^\dagger P_{IM,ii'} \\ &- \frac{1}{2}\sum_{ii'} \frac{\chi_{2,ii'}}{b^4} \sum_M :Q_{2M,ii'}^\dagger Q_{2M,ii'}: \\ &- \frac{1}{2}\sum_{ii'} \frac{\chi_{3,ii'}}{b^6} \sum_M :O_{3M,ii'}^\dagger O_{3M,ii'}: \\ &- \frac{1}{2}\sum_{ii'} \frac{\chi_{4,ii'}}{b^8} \sum_M :H_{4M,ii'}^\dagger H_{4M,ii'}: \\ &+ \sum_{a\le c,ii'} k_{mc}(ia,i'c) \sum_{1M} A_{1M}^\dagger(ia,i'c) A_{1M}(ia,i'c) \end{aligned} \quad (1)$$

Eq.(1) includes the single-particle Hamiltonian ($H_{\rm sp}$), the $J = 0$ and $J = 2$ pairing ($P_0^\dagger P_0$ and $P_2^\dagger P_2$), the quadrupole-quadrupole ($Q^\dagger Q$), the octupole-octupole ($O^\dagger O$), the hexadecapole-hexadecapole ($H^\dagger H$) terms, and the monopole corrections ($H_{\rm mc}$). In the pn representation, $P_{JM,ii'}^\dagger$ and $A_{JM}^\dagger(ia,i'b)$ are the pair operators, and $Q_{2M,ii'}^\dagger$, $O_{3M,ii'}^\dagger$, and $H_{4M,ii'}^\dagger$ are the quadrupole, octupole, and hexadecapole operators, respectively, in which i and i' are indices for proton or neutron. The constants $g_{J,ii'}$, $\chi_{2,ii'}$, $\chi_{3,ii'}$, $\chi_{4,ii'}$, and $k_{\rm mc}(ia,i'b)$ are the corresponding force strengths, and b is the harmonic-oscillator range parameter. The force strengths of the Hamiltonian are listed in Table 1. In Ref.[42], the monopole and multipole effects are examined carefully by using the generator-coordinate method. In this work, three monopole correction terms are incorporated to apply the interaction to Zr isotopes near A = 90:

$$\begin{aligned} Mc1 &\equiv k_{\rm mc}(\nu g_{7/2}, \nu g_{7/2}) = -0.9 \text{ MeV} \\ Mc2 &\equiv k_{\rm mc}(\pi g_{9/2}, \nu g_{7/2}) = -0.2 \text{ MeV} \\ Mc3 &\equiv k_{\rm mc}(\pi g_{9/2}, \nu s_{1/2}) = -0.07 \text{ MeV} \end{aligned} \quad (2)$$

Table 1. The two-body force strengths (in MeV).

ii'	$g_{0,ii'}$	$g_{2,ii'}$	$\chi_{2,ii'}$	$\chi_{3,ii'}$	$\chi_{4,ii'}$
pp	39	350	600	550	0.0014
nn	18	320	400	70	0.0008
np	0	0	200	0	0.0009

As shown in Fig. 1, their effects are demonstrated with adding the three monopole terms one by one. For easy comparison of calculations with the corresponding data, the difference factor is defined as the ratio of the theoretical value to the corresponding datum. After only considering Mc1, the bottom level $7/2^+$ shifts up obviously, while the level $5/2^+$ goes down as the ground state in both ^{91}Zr and ^{93}Zr. The terms Mc2 and Mc3 improve well the level $1/2^+$ of ^{91}Zr (^{93}Zr) with a difference factor 1.06 (0.98) by comparing with the columns "+Mc1" and "+Mc3". In ^{92}Zr (^{94}Zr), the levels 2^+ and 4^+ are affected slightly with monopole corrections, while the level 6^+ shifts up well with a difference factor 0.99 (0.92) by comparing with the columns "+Mc0" and "+Mc3". The second 0^+ and 2^+ of ^{92,94}Zr are improved very well in both excited energies and orders. The cross-subshell of was reported in Ref.[43]. As shown in Fig. 1, the proportion of cross-subshell Z = 40 is listed as WI/WO, which means the ratio of with and without orbit $\pi g_{9/2}$ up Z = 40. In low-lying levels, the cross-subshell share drops obviously by including monopole corrections.

III. RESULTS AND DISCUSSIONS

A. ^{91}Zr

As a stable single-neutron nucleus, ^{91}Zr attracts extensive researches for decades. Arroe and Mack studied the optical hyperfine structure of Zr firstly, and obtained the nuclear spin of 5/2 for ^{91}Zr [44]. The ground state $5/2^+$ is formed by coupling proton holes in the $p_{1/2}$ and $g_{9/2}$ orbits with a neutron particle in the $d_{5/2}$ orbital. The low-lying excited states $1/2^+$ and $7/2^+$ arise from coupling the same proton holes with a neutron particle in the $s_{1/2}$ and $d_{5/2}$ orbits, respectively. As shown in Fig. 2, the ground state $5/2^+$ has 49.17% of configuration $p_{1/2}^{-2}g_{9/2}^{-8}\nu d_{5/2}^1$ and 44.35% of configuration $\pi g_{9/2}^{-10}\nu d_{5/2}^1$ The main configurations of the excited states $1/2^+$ and $7/2^+$ are 50.63% $\pi p_{1/2}^{-2}g_{9/2}^{-8}\nu s_{1/2}^1$ and 77.54% $\pi p_{1/2}^{-2}g_{9/2}^{-8}\nu d_{5/2}^1$, with difference factors 1.06 and 1.007 respectively.

High-spin levels in ^{91}Zr have been studied by using

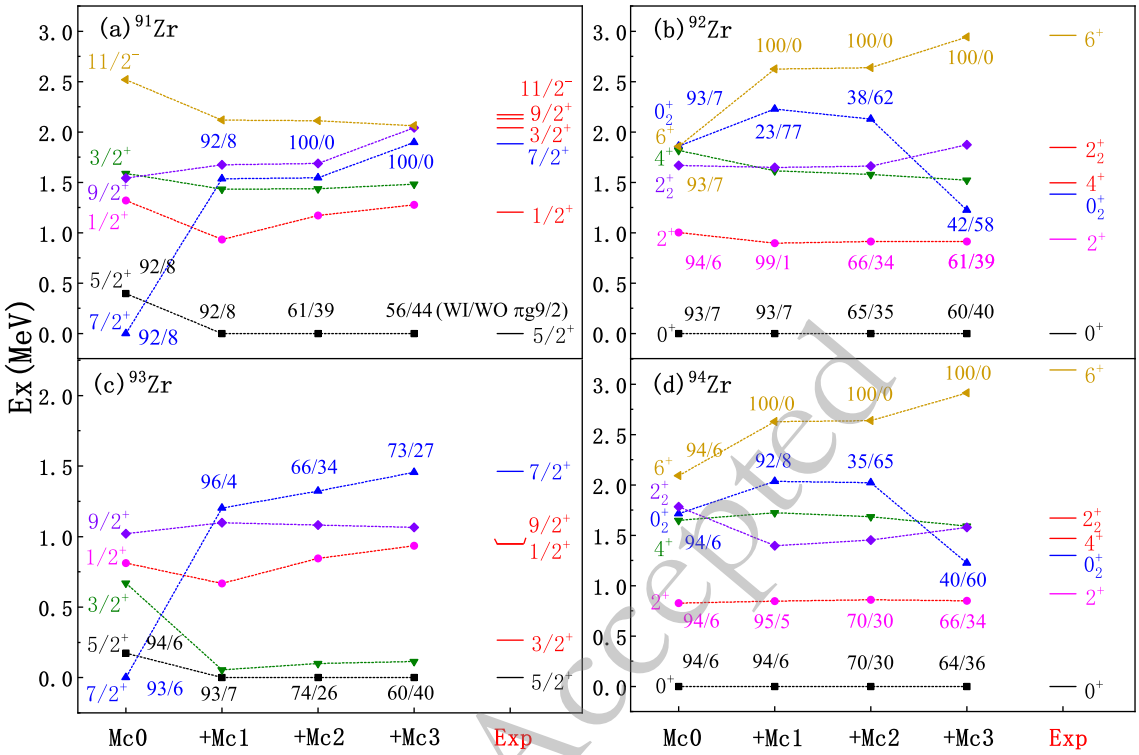

Fig. 1. (color online) Monopole effects in the low-lying levels of $^{91-94}$Zr, data from [29]. Label WI/WO is the ratio of with and without cross-subshell $\pi g_{9/2}$.

the reaction ^{88}Sr(^{6}Li,p2n)^{91}Zr, and the state $|(g_{9/2}p_{1/2}d_{5/2}),15/2^-\rangle$ is located at 2288 keV Ref.[45]. In Ref.[46], a $21/2^+$ state at 3167 keV was discovered using the reaction ^{88}Sr(^{6}Li,p2n)^{91}Zr. For the two data, the calculational levels $15/2^-$ and $21/2^+$ at 1951keV and 2870keV have the difference factors 0.85 and 0.9 respectively. The main configuration of the $15/2^-$ level is 96.85% of $\pi p^{-1}_{1/2}g^{-9}_{9/2}\nu d^{1}_{5/2}$. The main configuration of the $21/2^+$ level is 88.01% of $\pi p^{-2}_{1/2}g^{-8}_{9/2}\nu d^{1}_{5/2}$.

The level scheme of ^{91}Zr was extended with the newly $15/2^+$ and $19/2^+$ states at 3.41 MeV and 3.78 MeV in Ref.[48]. In calculations,the $15/2^+$ state at 3.01 MeV has a main configuration of $\pi p^{-2}_{1/2}g^{-8}_{9/2}\nu d^{1}_{5/2}$, with a difference factor 0.88. The first $19/2^+$ level at 3.047 MeV, and the second $19/2^+_2$ at 3.953 MeV. The $19/2^+_2$ state has a main configuration of $\pi p^{-1}_{1/2}g^{-9}_{9/2}\nu h^{1}_{11/2}$, with a difference factor 0.96. The present calculations extend the excited energy to $E_x \approx 10$ MeV. In calculations,the first $29/2^-$ level at 7.256 MeV, and the second $29/2^-_2$ at 7.393 MeV. The main configuration of $29/2^-_2$ is 96.61% of $\pi p^{-1}_{3/2}p^{-1}_{1/2}g^{-8}_{9/2}\nu h^{1}_{11/2}$, with a difference factor 1.034 by comparing with datum (29/2) at 7.663MeV. The configurations of $33/2^+$ and $35/2^+$ are 91.93% and 91.15% $\pi p^{-1}_{3/2}p^{-2}_{1/2}g^{-7}_{9/2}\nu h^{1}_{11/2}$, respectively. Their difference factors are 0.96 and 0.98 by comparing with data (33/2) and (35/2) at 9.129 and 9.462 MeV respectively. The ratio of with and without cross-subshell Z = 40 is added as WI/WO in Fig. 2. These quantitative proportions indicate that cross-subshell excitations dominate the low-excitation energy spectra, while the high-energy, high-spin portions of the spectra almost entirely originate from proton excitations across Z=40.

B. ^{92}Zr

In Ref. [50], the properties of the 2^+ states of ^{92}Zr were investigated though non-elastic electron scattering experiments under low momentum transfer conditions. It has been confirmed that the transitions to the 2^+_1 and 2^+_2 states primarily follow a monopole substructure mode(Fig. 3). The first excited state 2^+ at 911 keV has 41.68% of configuration of $\pi p^{-2}_{1/2}g^{-8}_{9/2}\nu d^{2}_{5/2}$, with a difference factor 0.97. The second 2^+_2 state at 1.874 MeV has 49.28% of configuration $\pi p^{-2}_{1/2}g^{-8}_{9/2}\nu d^{2}_{5/2}$, with a difference factor 1.01.In Ref. [51], this state was confirmed at 1.847 MeV by the $(n,n'\gamma)$ reaction.

The ground state 0^+ has two primary configurations: 43.59% of $\pi p^{-2}_{1/2}g^{-8}_{9/2}\nu d^{2}_{5/2}$ and 33.79% of $\pi g^{-10}_{9/2}\nu d^{2}_{5/2}$. The 0^+_2 level at 1224 keV has 48.79% of primary configuration $\pi g^{-10}_{9/2}\nu d^{2}_{5/2}$, with a difference factor 0.88. The first 4^+ level at 1.520 MeV agree with datum 1.495 MeV very well, with a difference factor 1.01. It has 49.09% of configuration $\pi p^{-2}_{1/2}g^{-8}_{9/2}\nu d^{2}_{5/2}$. The 6^+ and 8^+ states share the same dominant configuration $\pi p^{-2}_{1/2}g^{-8}_{9/2}\nu d^{2}_{5/2}$, 71.01% and 71.3% percentage respectively. The negative parity level 5^- at 2.014 MeV has a dominant configuration of $\pi p^{-1}_{1/2}g^{-9}_{9/2}\nu d^{2}_{5/2}$, 80.36%. This level was first proposed with

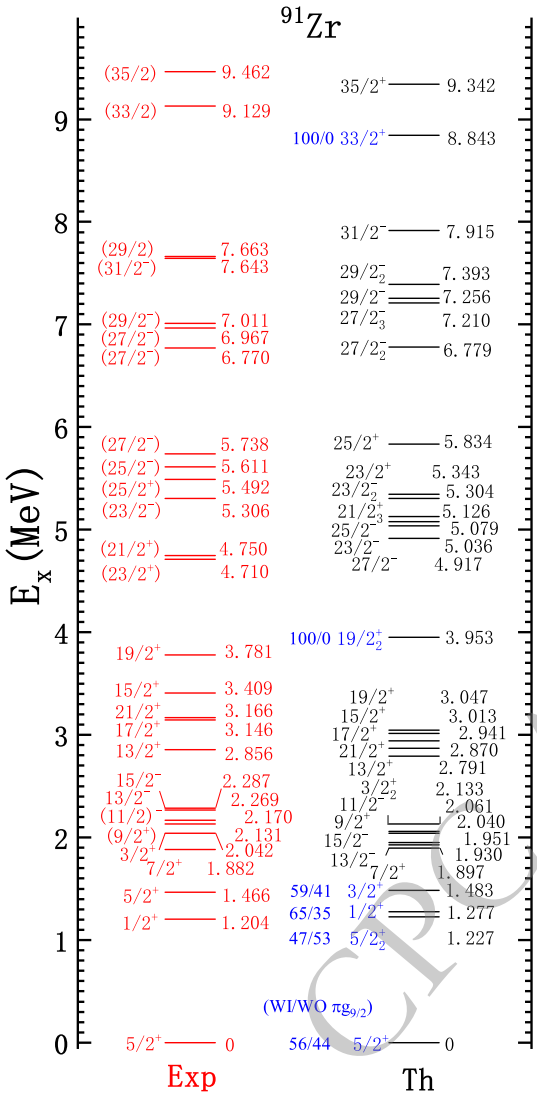

Fig. 2. (color online) Level spectra of ^{91}Zr, data from [44–48]. Label WI/WO is the ratio of with and without cross-subshell $\pi g_{9/2}$

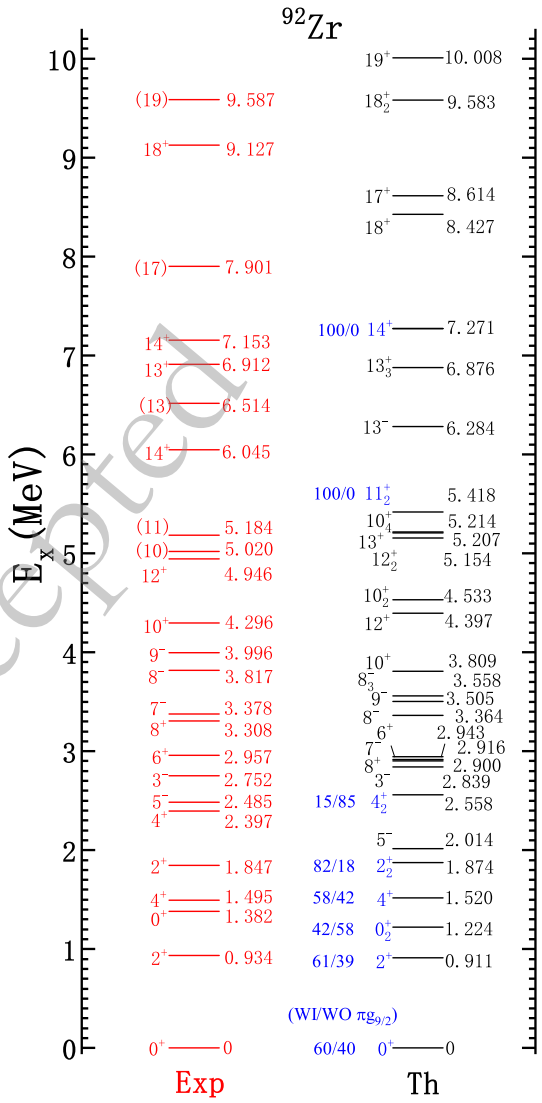

Fig. 3. (color online) Level spectra of ^{92}Zr, data from [49–55]. Label WI/WO is the ratio of with and without cross-subshell $\pi g_{9/2}$.

(p,p') angular distribution measurements by Dickens et al. in Ref. [52]. Brown et al.[53], based on negative coefficient measurements of the transition from 2485 keV to the 4^+ state at 1495 keV, suggested this level as J=3 or 5.

For high-spin states, Brown et al. conducted a study on the high spin states of ^{92}Zr through the ^{88}Sr(^{7}Li,p2n)^{92}Zr reaction, extending the spectra to 12^+ at 4947 keV [53]. In calculations, the first 12^+ level at 4.397 MeV, and the second 12^+ at 5.154 MeV. The 12^+_2 has 84.36% of configuration $\pi p^{-2}_{1/2} g^{-8}_{9/2} \nu d^2_{5/2}$, with a difference factor 1.04. Fotiades et al. [54] investigated the level structure of ^{92}Zr by the ^{24}Mg + ^{173}Yb reaction. The research extended the level scheme up to (18^+) state at $E_x \approx 9127$ keV. the first 18^+ level at 8.427 MeV, and the second 18^+ at 9.583 MeV.The 18^+_2 state has a difference factor of 1.04 by comparing with this datum. It has a dominant configuration of $\pi p^{-1}_{3/2} p^{-2}_{1/2} g^{-7}_{9/2} \nu d^1_{5/2} h^1_{11/2}$, 90.21% percentage. In 2025, the experimental research extend the excited energy of ^{92}Zr to $E_x \approx 10$ MeV with state (19) at 9.587 MeV[55]. The main configuration of level 19^+ is 90.82% of $\pi p^{-1}_{3/2} p^{-2}_{1/2} g^{-7}_{9/2} \nu d^1_{5/2} h^1_{11/2}$, with a difference factor 1.04 by comparing with datum (19) at 9.587 MeV.

C. ^{93}Zr

The ground state of ^{93}Zr was confirmed in Ref.[56]. Cohen and Chubinsky [57] performed nuclear reactions: pick-up ^{94}Zr(d,t)^{93}Zr and stripping ^{92}Zr(d,p)^{93}Zr, and proposed the $(d_{5/2})^n$ configuration dominating the low-lying level structure of ^{93}Zr. In calculations, the level $5/2^+$ has 43.84% of configuration $\pi p^{-2}_{1/2} g^{-8}_{9/2} \nu d^3_{5/2}$ and 33.62% of configuration $\pi g^{-10}_{9/2} \nu d^3_{5/2}$. In Ref.[58], a state $9/2^+$ was predicted at 1100 keV with the configuration $(d_{5/2})^3$. To

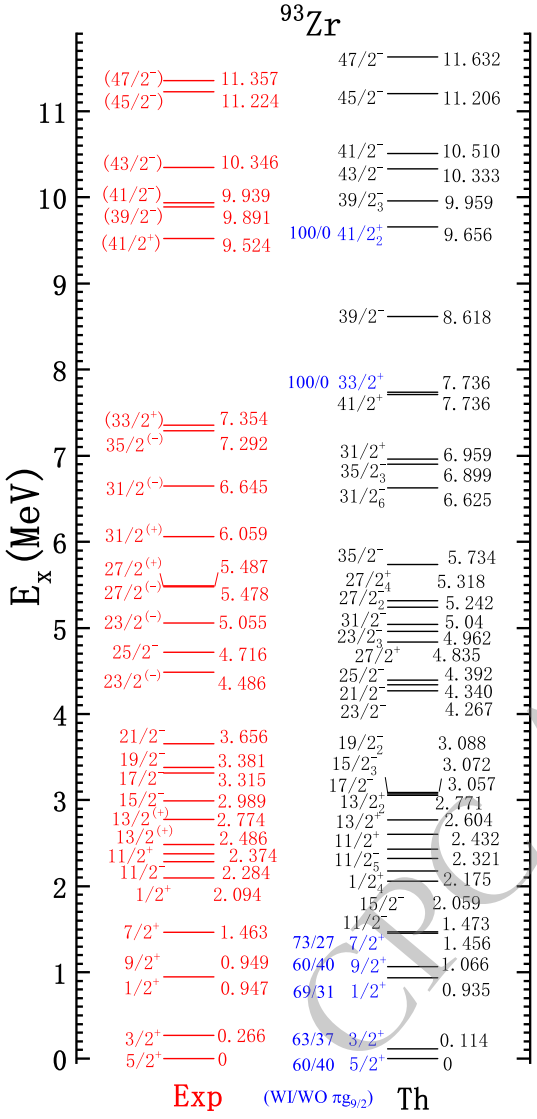

Fig. 4. (color online) Level spectra of ^{93}Zr, data from [54, 56, 60−62]. Label WI/WO is the ratio of with and without cross-subshell $\pi g_{9/2}$.

confirm this prediction, B. Arad et al. measured γ rays from the β decay of the fission product ^{93}Y using a Ge(Li) spectrometer, and tentatively established a level $9/2^+$ at 1167.7 keV [59]. The latest research[60] investigated the excited states of ^{93}Zr via the heavy-ion fusion-evaporation reaction, and identified the $9/2^+$ level at 949 keV. In this work, the level $9/2^+$ at 1.066 MeV has 47.04% of configuration $\pi p^{-2}_{1/2}g^{-8}_{9/2}\nu d^3_{5/2}$ and 36.93% of configuration $\pi g^{-10}_{9/2}\nu d^3_{5/2}$.

Besides low-lying levels, Ref. [54] extended the spectra of ^{93}Zr to about 4.5 MeV though the coincidence of γ transitions and their relative intensities. The spectrum of ^{93}Zr was extended to about 7 MeV via reaction ^{28}Si + ^{176}Yb, and the level at 4716.8 keV, which was assigned a spin-parity of $25/2^+$ for the first time [62]. However, in the latest article, the energy level at 4716 keV has been assigned as $25/2^-$, and the parity is determined to be negative. In calculations(4), the level $25/2^-$ at 4.392 MeV has 68.67% of configuration $\pi p^{-2}_{1/2}g^{-8}_{9/2}\nu d^2_{5/2}h^1_{11/2}$, with an difference factor 0.93. In research [60], the energy spectrum of ^{93}Zr was extended to $E \approx 12.5$ MeV with the spin-parity to $I^\pi = (47/2^-)$. In calculations, the level $47/2^-$ at 11.632 MeV has 85.05% of configuration $\pi p^{-1}_{3/2}p^{-2}_{1/2}g^{-7}_{9/2}\nu d^1_{5/2}h^2_{11/2}$, with a difference factor 1.02. The level $45/2^-$ at 11.206 MeV has 89.96% of configuration $\pi p^{-1}_{3/2}p^{-2}_{1/2}g^{-7}_{9/2}\nu d^1_{5/2}h^2_{11/2}$, and the difference factor is 0.99.

D. ^{94}Zr

The low-spin states of ^{94}Zr was investigated through the β-decay of ^{94}Y in Ref.[66, 67]. The 2^+_2 state at 1671.4 keV was determined via the $(n,n'\gamma)$ reaction [64]. Peters et al. [65] remeasured the energy of 1671 keV using the Doppler-shift attenuation method (DSAM) and the $(n,n'\gamma)$ reaction, which also reported the second 2^+ state at 1671 keV. As shown in Fig. 5, the ground state 0^+ has two primary configurations: $\pi p^{-2}_{1/2}g^{-8}_{9/2}\nu d^4_{5/2}$ (35.51%) and $\pi g^{-10}_{9/2}\nu d^4_{5/2}$ (24.67%). The level 2^+ at 0.849 MeV has 34.58% of configuration $\pi p^{-2}_{1/2}g^{-8}_{9/2}\nu d^4_{5/2}$, with a difference factor 0.92. The 2^+_2 state at 1579 keV has a difference factor 0.94, which has mixed configurations: 16.21% of $\pi p^{-2}_{1/2}g^{-8}_{9/2}\nu d^3_{5/2}s^1_{1/2}$, 13.02% of $\pi p^{-2}_{1/2}g^{-8}_{9/2}\nu d^4_{5/2}$, and 8.97% of $\pi p^{-2}_{1/2}g^{-8}_{9/2}\nu d^3_{5/2}d^1_{3/2}$. The level 4^+ at 1.592 MeV has 43.86% of configuration $\pi p^{-2}_{1/2}g^{-8}_{9/2}\nu d^4_{5/2}$, with a difference factor 1.08. The level 4^+_2 at 2.251 Mev has 22.42% of $\pi p^{-2}_{1/2}g^{-8}_{9/2}\nu d^3_{5/2}d^1_{3/2}$ configuration, with a difference factor 0.96.

For the high-spin states, Ref. [54] observed some data from 4812 KeV to 7791 KeV via the decay of the compound nucleus ^{197}Pb produced by a ^{24}Mg beam at 134.5 MeV. Based on this research,via detecting the prompt γ-rays on the EUROGAM II and EUROBALL arrays, Pantelica et al. [62] assigned spins and parities of states (12^+) at 4813.8 keV, (11^+) at 5492.9 keV, (12^+_2) at 5806.9 keV, and (13^+) at 6009.51 keV, as well as spin-assigned states (14), (15) and (16) listed in the top of Fig. 5. In calculations(5), the first 12^+ level at 4.549 MeV has a difference factor 0.942 by comparing datum 4.813 MeV. The 12^+_3 at 4.829 MeV reproduce well the datum 4.813 MeV with a difference factor 1.003, which has 68.78% of $\pi p^{-1}_{1/2}g^{-9}_{9/2}\nu d^3_{5/2}h^1_{11/2}$ configuration. For the datum (14) at 6.374 MeV, the first 14^+ level at 5.787 MeV has 69.09% of $\pi p^{-1}_{1/2}g^{-9}_{9/2}\nu d^3_{5/2}h^1_{11/2}$ configuration. The level 14^+_3 at 6.131MeV has 45.84% of $\pi g^{-10}_{9/2}\nu d^2_{5/2}h^2_{11/2}$ configuration, with a difference factor 0.96. The first 15^+ level at 5.849 MeV has 69.93% of $p^{-1}_{1/2}g^{-9}_{9/2}\nu d^3_{5/2}h^1_{11/2}$ configuration The level 15^+_2 at 7.070 MeV has a difference factor 1.001 by comparing with datum (15) at 7.058 MeV, which has 85.84% of $\pi p^{-1}_{1/2}g^{-9}_{9/2}\nu d^2_{5/2}h^1_{11/2}d^1_{3/2}$ configuration. The first 16^+ level at 7.125 MeV has 56.71% $\pi p^{-2}_{1/2}g^{-8}_{9/2}\nu d^2_{5/2}h^2_{11/2}$ configuration. The level 16^+_4 at 7.619 MeV reproduce

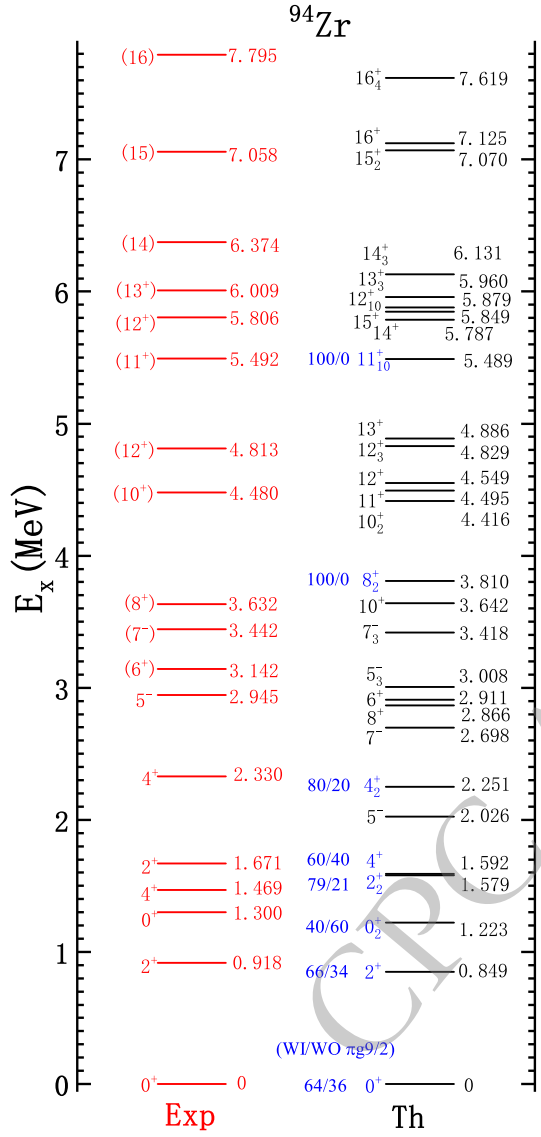

Fig. 5. (color online) Level spectra of ^{94}Zr, data from [54, 62−65]. Label WI/WO is the ratio of with and without cross-subshell $\pi g_{9/2}$

well the datum 7.795 MeV with a difference factor 0.97, which has 65.32% of $\pi g_{9/2}^{-10}\nu d_{5/2}^2 h_{11/2}^2$ configuration.

E. Electromagnetic Transitions

Electric quadrupole transitions reflect the degree of collective nuclear deformation, which is described by the transition probability $B(E2)$. The transition probabilities are stringent tests for the wave function of energy levels. The isomerism was discussed with lifetimes in the south-eastern vicinity of ^{208}Pb[68].

In Tab. 2, we list the $B(E2)$ values with lifetimes.

The value 3.68 W.u. of $B(E2;1/2^+ \to 5/2^+)$ has a difference factor 0.24 by comparing with datum 15 W.u. of ^{91}Zr. The value 2.03 W.u. from the second $1/2^+$ level has a difference factor 0.78 with datum 1.6 W.u. The E2 values from $7/2^+$ and $9/2^+$ to the ground state reproduce well the data 7.7 and 4.2 W.u. In ^{92}Zr, the value 2.1 W.u. of $B(E2;2^+ \to 0^+)$ has a difference factor 0.32 by comparing with datum 6.4 W.u. The value 3.79 W.u. from the second 2^+ level has a nice difference factor 1.02 with datum 3.7 W.u.

In ^{93}Zr, the value 4.45 W.u. of $B(E2;3/2^+ \to 5/2^+)$ has a difference factor 0.63 by comparing with datum 7(6) W.u. The $B(E2)$ value from second $3/2^+$ to the ground state $5/2^+$ is 0.73 W.u. For other $B(E2)$ transitions, no more experimentally measured values are available, and we have theoretically calculated those from several low-lying excited states to the ground state. For example, the value of $B(E2;1/2^+ \to 5/2^+)$ is 1.61 W.u. and the second $1/2^+$ state to the ground state $5/2^+$ is 3.71 W.u. The value of $B(E2;9/2^+ \to 5/2^+)$ is 1.73 W.u. and the second $1/2^+$ state to the ground state $5/2^+$ is 4.39 W.u.

In ^{94}Zr, the $B(E2;2_1^+ \to 0_1^+)$ was obtained as 4.9(11) W.u. via the (n, n′) reaction in the Doppler Shift Attenuation Method (DSAM)[69]. As shown in Table 2,the corresponding value is 2.57 W.u. with a difference factor 0.52. The $B(E2)$ value from second 2^+ to the ground state 0^+ is 3.27 W.u., which has a difference factor 0.83 with the datum 3.9 W.u. The value 0.55 W.u. from 4^+ to 2^+ reproduces very well the corresponding datum 0.88(23). Several experimental $B(E2)$ transition probabilities have been observed to significantly exceed calculations. Notable examples include the $B(E2;3/2^+ \to 5/2^+) = 59(6)$ W.u. in ^{91}Zr, the $B(E2;10_1^+ \to 8_1^+) = 31^{+5}_{-4}$ W.u in ^{92}Zr, and the $B(E2;4_2^+ \to 2_2^+) = 34^{+10}_{-7}$ W.u. in ^{94}Zr. As reported in Ref. [69], the $B(E2)$ values in ^{94}Zr provide direct evidence for a consistent picture of shape coexistence. Furthermore, Ref. [70] reports the large $B(E2)$ value in ^{92}Zr and proposes, within a phenomenological deformed rotor model, that the observed nuclear collectivity may originate from a coexisting deformed structure. The consistently enhanced $B(E2)$ values across these Zr isotopes indicate the nuclear collectivity in this region, while a truncated model space severely limits the ability of the shell model to describe nuclear collective effects.

IV. SUMMARY

In this work, a suitable interaction is designed for investigating the level structure of Zr isotopes over N = 50 shell. The interaction is composed by the pairing-plus-multipole force and monopole correction terms. Three monopole correction terms are added to modify the single particle states of ^{132}Sn to suit the low-lying states of ^{91}Zr close to the N = 50 shell. The present interaction describes well the level structure of $^{91-94}$Zr in both low-lying and high-spin excitations.

The excited states of ^{91}Zr extend to about 10 MeV with spin up to $J = 35/2$. By including three monopole

Table 2. Electric quadrupole transitions [29, 64, 69–71].

^{Z}X	Transition(W.u.)	τL	Exp.	τ (ps)	Th.	τ (ps)
^{91}Zr	$1/2^+ \to 5/2^+$	E2	15(4)	0.89	3.68	1.86
	$1/2^+_2 \to 5/2^+$	E2	1.6^{+5}_{-8}	0.19	2.03	0.26
	$7/2^+ \to 5/2^+$	E2	7.7(13)	0.109	4.93	0.13
	$7/2^+_2 \to 5/2^+$	E2	1.15^{+21}_{-32}	$0.48^{+13}_{-8.7}$	0.09	0.81
	$3/2^+ \to 5/2^+$	E2	59(6)	0.016	0.68	0.005
	$3/2^+_2 \to 5/2^+$	E2			3.32	
	$3/2^+_3 \to 5/2^+$	E2		0.024	0.01	0.09
	$9/2^+ \to 5/2^+$	E2	4.2(6)	0.163	4.28	0.15
	$(13/2)^+ \to (9/2^+)$	E2	> 0.0079		7.73	
	$(13/2)^+_2 \to (9/2^+)$	E2			0.87	
	$(17/2)^+ \to (13/2^+)$	E2	> 0.19		5.48	
	$(17/2)^+_2 \to (13/2^+)$	E2			0.37	
^{92}Zr	$2^+ \to 0^+$	E2	$6.4^{+0.6}_{-0.5}$[71]	7.21(58)	2.1	1.727
	$2^+_2 \to 0^+$	E2	3.4(4)[71]	0.138(14)	3.79	0.25
	$2^+_3 \to 0^+$	E2	< 0.005[71]	> 1.1	0.19	2.27
	$2^+_4 \to 0^+$	E2	0.048(7)	0.092(10)	0.36	1.01
	$2^+_5 \to 0^+$	E2			0.001	
	$4^+ \to 2^+$	E2	4.05(11)[71]	0.147(4)	1.26	2.15
	$4^+_2 \to 2^+$	E2	6.1(8)[71]	0.215(23)	3.1	0.58
	$4^+_3 \to 2^+$	E2			0.06	
	$4^- \to 5^-$	E2	< 0.3			
	$4^-_2 \to 5^-$	E2			0.07	
	$10^+ \to 8^+$	E2	31^{+5}_{-4}[70]		2.14	
^{93}Zr	$3/2^+ \to 5/2^+$	E2	7(6)	2092(7)	4.45	13870
	$3/2^+_2 \to 5/2^+$	E2			0.73	
	$3/2^+_3 \to 5/2^+$	E2			0.57	
	$3/2^+_4 \to 5/2^+$	E2			1.78	
	$1/2^+ \to 5/2^+$	E2			1.61	
	$1/2^+_2 \to 5/2^+$	E2			3.71	
	$1/2^+_3 \to 5/2^+$	E2			0.002	
	$1/2^+_4 \to 5/2^+$	E2			0.67	
	$9/2^+ \to 5/2^+$	E2			1.73	
	$9/2^+_2 \to 5/2^+$	E2			4.39	
	$9/2^+_3 \to 5/2^+$	E2			0.09	
	$9/2^+_4 \to 5/2^+$	E2			0.06	
^{94}Zr	$2^+ \to 0^+$	E2	4.9(11)[69]	9.9(21)	2.57	19.7
	$2^+_2 \to 0^+$	E2	3.9(3)[69]	$3.68^{+0.027}_{-0.023}$	3.27	0.69
	$2^+_3 \to 0^+$	E2			1.42	
	$2^+_2 \to 0^+_2$	E2	19(2)[69]		1.85	
	$2^+_3 \to 0^+_2$	E2	0.04(5)[64]		3.38	
	$2^+_4 \to 0^+_2$	E2			0.04	

Continued on next page

Table 2-continued from previous page

^{Z}X	Transition(W.u.)	τL	Exp.	τ (ps)	Th.	τ (ps)
	$0_2^+ \to 2^+$	E2	9.3(4)[69]		1.53	
	$0_3^+ \to 2^+$	E2			0.04	
	$0_4^+ \to 2^+$	E2			2.23	
	$4^+ \to 2^+$	E2	0.88(23)[69]	721(19)	0.55	177
	$4_2^+ \to 2^+$	E2	13^{+4}_{-7}[69]	$0.42^{+0.20}_{-0.11}$	4.69	0.85
	$4_3^+ \to 2^+$	E2			0.74	
	$4_2^+ \to 2_2^+$	E2	34^{+10}_{-7}[69]		3.94	
	$4_3^+ \to 2_2^+$	E2			1.67	

correction terms, the energy ordering and positions of low-lying levels (e.g., $5/2^+$, $1/2^+$, $7/2^+$, and $11/2^-$) are significantly improved, bringing them into good agreement with experimental values. The model also satisfactorily reproduces other high-spin states (e.g., $29/2^-$, $33/2^+$, $35/2^+$). Specifically, the $29/2_2^-$ state have the difference factor 0.96, which are coupled by orbits $\pi p_{3/2}$, $\pi p_{1/2}$, $\pi g_{9/2}$ and $\nu g_{9/2}$. The $33/2^+$ and $35/2^+$ states have the difference factors 0.96 and 0.98, which are coupled by orbits $\pi p_{3/2}$, $\pi p_{1/2}$, $\pi g_{9/2}$ and $h_{11/2}$. The excited levels of ^{92}Zr are well explained up to about 10 MeV with spin $J = 19$. For examples, the low-lying states 2^+, 4^+ and 6^+ reproduce well the corresponding data with difference factors 0.97, 1.01, and 0.99 respectively, which are coupled by orbits $\pi p_{1/2}$, $\pi g_{9/2}$ and $\nu d_{5/2}$. The high-spin levels 12_2^+ and 18_2^+ show the same difference factors 1.04, which are coupled by the orbits $\pi p_{1/2}$, $\pi g_{9/2}$, $\nu d_{5/2}$ and $\nu h_{11/2}$.

The level spectra of ^{93}Zr are reproduced well with excited energy more than 11 MeV. For example, the low-lying levels $1/2^+$, $9/2^+$ and $13/2^+$ have the difference factors 0.98, 1.12 and 1.04 respectively, which are coupled by orbits $\pi p_{1/2}$, $\pi g_{9/2}$, $\nu d_{5/2}$ and $\nu s_{1/2}$. The high levels $43/2^-$, $45/2^-$, and $47/2^-$ have the difference factors 0.99, 0.99 and 1.02 respectively, which are coupled by the orbits $\pi p_{1/2}$, $\pi g_{9/2}$, $\nu d_{5/2}$ and $\nu h_{11/2}$. The level spectra of ^{94}Zr are investigated up to about 8 MeV with spin $J = 16$. The low-lying states 2^+, 4^+, and 6^+ have the difference factors 0.92, 1.08 and 0.92 respectively, which are coupled by orbits $\pi p_{1/2}$, $\pi g_{9/2}$ and $\nu d_{5/2}$. The high spin states 14_3^+, 15_2^+ and 16_4^+ have the difference factors 0.96, 1.001 and 0.97 respectively, which are coupled by the orbits $\pi p_{1/2}$, $\pi g_{9/2}$, $\nu d_{5/2}$, $\nu h_{11/2}$ and $\nu d_{3/2}$.

The spectra of $^{91-94}$Zr are investigated in both low-lying and high-spin excitations, and their wave functions are further tested by comparing the electromagnetic transitions probabilities with given $B(E2)$ data. The calculations provide systematic predictions and configuration interpretations for the high-spin states of Zr isotopes. The well performance in both spectra and transitions probabilities makes the predicting calculations of the present interaction more dependable to be referred in further experimental researches of Zr isotopes.

References

[1] M. Quinn, A. Aprahamian, J. Pereira, *et al.*, Phys. Rev. C **85**, 035807 (2012)
[2] M. P. Reiter, S. Ayet San Andrés, S. Nikas, *et al.*, Phys. Rev. C **101**, 025803 (2020)
[3] R. Yokoyama, R. Grzywacz, B. C. Rasco, *et al.*, Phys. Rev. C **100**, 031302 (2019)
[4] C. Fougères, M. L. Avila, H. Jayatissa, *et al.*, Phys. Rev. C **109**, 065805 (2024)
[5] S. Han-Feng, Z. Bo, Z. Jiang, *et al.*, Chin. Phys. Lett. **20**, 2084 (2003)
[6] A. Banu, E. G. Meekins, J. A. Silano, *et al.*, Phys. Rev. C **99**, 025802 (2019)
[7] A. Spyrou, S. J. Quinn, A. Simon, *et al.*, Phys. Rev. C **88**, 045802 (2013)
[8] M. Beard, S. Frauendorf, B. Kämpfer, *et al.*, Phys. Rev. C **85**, 065808 (2012)
[9] S.-H. Cheng, J. Wen, L.-G. Cao, *et al.*, Chinese Physics C **47**, 024102 (2023)
[10] Y. Zheng, G. d. France, X.-H. Zhou, *et al.*, Chinese Physics C **44**, 024002 (2020)
[11] H. Wang, K.-Y. Ma, Y.-H. Wu, *et al.*, Chinese Physics C **45**, 014001 (2021)
[12] Y.-F. Lv, J.-B. Lu, G.-L. Zhang, *et al.*, Chinese Physics C **43**, 104102 (2019)
[13] B. Sun, F. Montes, L. S. Geng, *et al.*, Phys. Rev. C **78**, 025806 (2008)
[14] C. Izzo, J. Bergmann, K. A. Dietrich, *et al.*, Phys. Rev. C **103**, 025811 (2021)
[15] P. T. Hosmer, H. Schatz, A. Aprahamian, *et al.*, Phys. Rev. Lett. **94**, 112501 (2005)
[16] M. Madurga, R. Surman, I. N. Borzov, *et al.*, Phys. Rev. Lett. **109**, 112501 (2012)
[17] P. Hosmer, H. Schatz, A. Aprahamian, *et al.*, Phys. Rev. C **82**, 025806 (2010)
[18] G. Tagliente, P. M. Milazzo, K. Fujii, *et al.*, Phys. Rev. C **84**, 015801 (2011)

[19] A. Couture, R. F. Casten, R. B. Cakirli, Phys. Rev. C **104**, 054608 (2021)
[20] C. Freiburghaus, S. Rosswog, F.-K. Thielemann, The Astrophysical Journal **525**, L121 (1999)
[21] R. Surman, G. C. McLaughlin, M. Ruffert, *et al*., The Astrophysical Journal **679**, L117 (2008)
[22] S.-i. Fujimoto, K. Kotake, S. Yamada, *et al*., The Astrophysical Journal **644**, 1040 (2006)
[23] G. Tagliente, K. Fujii, P. M. Milazzo, *et al*., Phys. Rev. C **77**, 035802 (2008)
[24] G. Tagliente, P. M. Milazzo, K. Fujii, *et al*., Phys. Rev. C **78**, 045804 (2008)
[25] G. Tagliente, P. M. Milazzo, K. Fujii, *et al*., Phys. Rev. C **81**, 055801 (2010)
[26] P. Rudling, R. Adamson, in: Materials Ageing and Degradation in Light Water Reactors, edited by K. Murty, Woodhead Publishing, Woodhead Publishing Series in Energy, 246–283 (2013)
[27] K. Kolos, A. Hennessy, N. Scielzo, *et al*., Nuclear Instruments and Methods in Physics Research Section A: Accelerators, Spectrometers, Detectors and Associated Equipment (2021) **1000**, 165240
[28] A. TAKIBAEV, M. SAITO, V. ARTISYUK, *et al*., Journal of Nuclear Science and Technology **37**, 870 (2000)
[29] https://www.nndc.bnl.gov/ensdf/
[30] T. Sumikama, K. Yoshinaga, H. Watanabe, *et al*., Phys. Rev. Lett. **106**, 202501 (2011)
[31] S. Miyahara, H. Nakada, Phys. Rev. C **98**, 064318 (2018)
[32] P. Banerjee, S. Ganguly, M. K. Pradhan, *et al*., Phys. Rev. C **98**, 034320 (2018)
[33] E. V. Mardyban, E. A. Kolganova, T. M. Shneidman, *et al*., Phys. Rev. C **105**, 024321 (2022)
[34] W. Witt, V. Werner, N. Pietralla, *et al*., Phys. Rev. C **98**, 041302 (2018)
[35] J. E. García-Ramos, K. Heyde, Phys. Rev. C **100**, 044315 (2019)
[36] A. Chakraborty, E. E. Peters, B. P. Crider, *et al*., Phys. Rev. Lett. **110**, 022504 (2013)
[37] Z. Ge, M. Reponen, T. Eronen, *et al*., Phys. Rev. Lett. **133**, 132503 (2024)
[38] H. B. Lv, G. X. Zhang, B. S. Cai, *et al*., Phys. Rev. C **111**, 044311 (2025)
[39] T. R. Routray, P. Bano, M. Anguiano, *et al*., Phys. Rev. C **104**, L011302 (2021)
[40] B. Brown, W. Rae, Nucl. Data Sheets **120**, 115 (2014)
[41] H.-K. Wang, Y. Sun, H. Jin, *et al*., Phys. Rev. C **88**, 054310 (2013)
[42] C.-F. Jiao, C.-X. Yuan, Nuclear Science and Techniques **36**, 202 (2025)
[43] Z.-X. Wang, G.-X. Zhang, W. Jiang, *et al*., Nuclear Science and Techniques **36**, 179 (2025)
[44] O. H. Arroe, J. E. Mack, Phys. Rev. **76**, 873 (1949)
[45] B. A. Brown, P. M. S. Lesser, D. B. Fossan, Phys. Rev. Lett. **34**, 161 (1975)
[46] B. A. Brown, P. M. S. Lesser, D. B. Fossan, Phys. Rev. C **13**, 1900 (1976)
[47] C. M. Baglin, Nuclear Data Sheets **114**, 1293 (2013)
[48] Z. G. Wang, M. L. Liu, Y. H. Zhang, *et al*., Phys. Rev. C **89**, 044308 (2014)
[49] C. M. Baglin, Nuclear Data Sheets **113**, 2187 (2012)
[50] A. S. Obeid, O. Burda, M. Chernykh, *et al*., Phys. Rev. C **87**, 014337 (2013)
[51] C. Fransen, V. Werner, D. Bandyopadhyay, *et al*., Phys. Rev. C **71**, 054304 (2005)
[52] J. K. Dickens, E. Eichler, G. R. Satchler, Phys. Rev. **168**, 1355 (1968)
[53] B. A. Brown, D. B. Fossan, P. M. S. Lesser, *et al*., Phys. Rev. C **14**, 602 (1976)
[54] N. Fotiades, J. A. Cizewski, J. A. Becker, *et al*., Phys. Rev. C **65**, 044303 (2002)
[55] Y. Hao, Z. Ren, J.-B. Lu, *et al*., Phys. Rev. C **111**, 034312 (2025)
[56] J. Knight, D. Hoffman, B. Dropesky, *et al*., Journal of Inorganic and Nuclear Chemistry **10**, 183 (1959)
[57] B. L. Cohen, O. V. Chubinsky, Phys. Rev. **131**, 2184 (1963)
[58] I. Talm, Phys. Rev. **126**, 2116 (1962)
[59] B. Arad, J. Boulter, W. Prestwich, *et al*., Nuclear Physics A **131**, 137 (1969)
[60] S. X. Guan, C. B. Li, Y. Zheng, *et al*., Phys. Rev. C **112**, 014304 (2025)
[61] C. M. Baglin, Nuclear Data Sheets **112**, 1163 (2011)
[62] D. Pantelica, I. G. Stefan, N. Nica, *et al*., Phys. Rev. C **72**, 024304 (2005)
[63] D. Abriola, A. Sonzogni, Nuclear Data Sheets **107**, 2423 (2006)
[64] E. Elhami, J. N. Orce, S. Mukhopadhyay, *et al*., Phys. Rev. C **75**, 011301 (2007)
[65] E. E. Peters, A. Chakraborty, B. P. Crider, *et al*., Phys. Rev. C **88**, 024317 (2013)
[66] S. Hontzeas, D. Marsden, Nuclear Physics A **179**, 193 (1972)
[67] J. B. Ball, R. L. Auble, P. G. Roos, Phys. Rev. C **4**, 196 (1971)
[68] M. Liu, C. Yuan, G. Zhang, *et al*., Science China Physics, Mechanics & Astronomy **68**, 122011 (2025)
[69] A. Chakraborty, E. E. Peters, B. P. Crider, *et al*., Phys. Rev. Lett. **110**, 022504 (2013)
[70] M. Sugawara, Y. Toh, M. Koizumi, *et al*., Phys. Rev. C **96**, 024314 (2017)
[71] C. Fransen, V. Werner, D. Bandyopadhyay, *et al*., Phys. Rev. C **71**, 054304 (2005)